AIAA JOURNAL
Vol. 32, No. 11, November 1994

Droplet Dispersion and Ejection Processes in Two-Phase Boundary Layer

M. R. Wang* and D. Y. Huang†
National Cheng Kung University, Tainan, Taiwan 70101, Republic of China

Measurements of the droplet transport property in the two-phase turbulent boundary layer were performed in a vertical downward duct by a phase Doppler particle analyzer (PDPA). The test Reynolds number based on the hydraulic diameter (i.e., D_h = 100 mm) is 70,100 and the drop size range is from 3.1 μm to 110 μm. Results reveal that the existence of drops in the boundary layer has significant effects on both the velocity profile and the turbulence intensities of the flow. Measurements show that flow characteristics are controlled by the droplet transport process, i.e., the dispersion of droplets from the freestream to the boundary-layer region and the ejection of droplets from the boundary-layer region to the freestream. Analysis of the data indicates that the normalized number density profiles in the boundary-layer region are linear and collapse for all drop size classes. The linear coefficient of the normalized number density is 1.17 ± 0.15. The data for the dispersion coefficients are also provided in this paper. The slopes of the dispersion coefficients for the larger drops (i.e., 50 and 80 μm) and for the smaller drops (i.e., 20 μm) are 22.66 and 15.75, respectively. These data are very useful in the numeric simulation of the spray flow. Analysis on the experiments data also shows that the droplet ejection factor is 10 and 6% for 20- and 30-μm drops, respectively. This implies that modeling of the two-phase boundary-layer problem should consider the droplet ejection process in the small size range.

Nomenclature

A_p = measuring probe area
D_h = hydraulic diameter
D_p = droplet dispersion coefficient
d_p = droplet diameter
l_e = characteristic length of the most energetic eddy without drop loading
ND = number density
NF = net number flux of droplets toward Y direction
N_i = total number of drops sampled for a specified drop size i
$n_i(V^+)$ = number of drops with a positive transverse velocity of a specified drop size i
$n_i(V^-)$ = number of drops with a negative transverse velocity of a specified drop size i
$P(V^+)$ = percentage of droplets with a positive transverse velocity
$P_{BL}(V^+)$ = $P(V^+)$ in the boundary layer
$P_f(V^+)$ = $P(V^+)$ in the freestream
Re_{D_h} = Reynolds number based on the hydraulic diameter
Re_θ = Reynolds number based on the momentum thickness
t = total sampling time
U_f = gas streamwise velocity at the freestream
U_g = gas streamwise velocity
U_p = particle streamwise velocity
u' = streamwise velocity fluctuation
V = transverse velocity
V_{disp} = droplet dispersion velocity
v' = transverse velocity fluctuation
X = streamwise coordinate
Y = transverse coordinate
Γ = linear coefficient of normalized number density
Δd_i = size interval of each drop size i
δ = boundary-layer thickness
Ψ_L = Droplet ejection factor in the boundary layer

Received June 23, 1993; revision received April 14, 1994; accepted for publication May 16, 1994.

*Associate Professor, Institute of Aeronautics and Astronautics. Member AIAA.
†Graduate Assistant, Institute of Aeronautics and Astronautics.

I. Introduction

THE phenomenon of turbulent fluid flows when loading liquid droplets is complex and is relatively unexplored. The study of the two-phase suspension flow is important in many practical industrial applications, for example, the mixing in spray combustion, the deposition of droplets on a wall, and so on. The distinct inertia of the droplet phase and the gas phase in the two-phase suspension flow normally gives rise to a significant velocity difference between the two.[18] Such phenomenon, in turn, influences the mass, momentum, and energy transport processes in the two-phase turbulent flow. The transport phenomenon in the boundary layer of a single phase flow is found to be enhanced by the bursting process,[13] which causes ejection from the wall region to the main stream and is followed by an insweep from the higher momentum region to the lower momentum region.

It has been known that a solid wall or free surface would suppress the normal components of turbulent fluctuation due to kinematic constraint. The solid wall or free surface would also generate an organized structure if mean shear is imposed on it. The phenomenon of alternating high-speed and low-speed motions near the solid boundary was first observed by Kline et al.[8] In Ref. 8 it was found that the well-organized spatially and temporally dependent motions within the viscous sublayer lead to the formation of low-speed streaks in the near wall region. This process was further identified by Blackwelder and Eckelmann[3] in 1979. The low-speed streaks interact with the outer portions of the flow through a process of gradual lift up, followed by sudden oscillation and the ejection of low-momentum fluid from the wall region to the main stream. This is then followed by an insweep of high-momentum fluid into the wall region. A series of these processes constitutes the so-called "bursting process." Burst structures in the near wall region of the turbulent flow are responsible for momentum transport from the wall. Quantitative measurements of the time scales associated with the burst events and techniques to detect an ejection structure were successfully developed by Lushite and Tiederman.[10] This bursting process is also equivalent to near-wall turbulence kinetic energy production and the Reynolds stress production processes. These results were further confirmed by Kim et al.[7]

The transport mechanism of the bursting processes for particles in the two-phase flow was further studied by Rashidi et al.[12] In Ref. 12 it was found that the low-speed streak observed near the wall is formed between pairs of longitudinal counter-rotating vor-

tices. These vortices are elongated in the flow direction and are separated in the spanwise direction. As particles are introduced into the flow, most of the particles accumulate in the low-speed streak of the wall structure. These particles are then lifted up (depending on their size and density) by the inclined vortex loops in the wall regions and are then ejected into the bulk flow. The ejected particles, having a density slightly greater than fluid, eventually turn back to the wall region. Some of the particles which have returned to the wall region, in turn, encounter wall ejections which are already in progress. These particles are lifted up before reaching the wall region. The bursting process repeats itself thus causing the transport of particles in the flow direction.

Roger and Eaton[14] studied the response of solid particles to turbulence modulation in a vertical upward flat plate turbulent boundary layer. Measurements were made under zero and adverse pressure gradient at the particle mass loading of both 2 and 20%. Glass beads of either 50 or 90 μm were uniformly loaded into the air flow at flow Reynolds number based on a hydraulic diameter of 66,500. The results showed that the mean velocity of 90-μm particles lag behind the 50-μm particles in the streamwise direction, and their velocities are much lower than that of the gas flow in the entire boundary layer. However, it is clear that the measured values of the streamwise velocity fluctuation for both particle sizes are nearly identical to that of the gas flow. This indicates that the particles are able to follow all of the fluctuations of the flow in the streamwise direction. On the other hand, however, the turbulent intensity of the particles in the normal direction is strongly attenuated, i.e., the intensity is much lower than that of the fluid. Analysis of the power spectra showed that the turbulent energy of the gas phase in the normal direction is higher in a high frequency range when compared to that in the streamwise direction. This indicates that the particles do not closely follow the fluid fluctuations in the transverse direction.

Rashidi et al.[12] also studied particle-turbulence interaction in a boundary layer. A series of experiments based on various particle sizes, particle densities, particle loading rates, and flow Reynolds numbers has been performed. The solid particles, i.e., spherical polystyrene with sizes ranging from 120 to 1100 μm, and spherical glass beads of 88 μm, were loaded into the water flow. The flow Reynolds number based on the flow depth varies from 2500 to 7500. The results showed that the larger polystyrene particles (i.e., 1100 μm) cause an increase in the number of ejections, giving rise to an increase in the measured values of the turbulent intensities and the Reynolds stresses. On the other hand, the use of smaller polystyrene particles (i.e., 120 μm) brings about a decrease in the number of ejections, causing a decrease in the measured turbulence intensities and the Reynolds stresses. It was also found that these effects are enhanced as the particle loading is increased. Furthermore, measurements show that the change of the bursting frequency and the mean streak spacing is insignificant when the particle loading increases.

Efforts were also made to investigate the effects of particle size on turbulence modulation for the carrier phase.[5,6,9,14–16] Tsuji and Morikawa[15] and Tsuji et al.[16] investigated the effects of particle size on turbulent intensities in both horizontal and vertical pipes for two-phase flow loading with solid particles. The results revealed that small particles, $d_p = 200$ μm, $Re_p \approx \mathcal{O}(0.10)$ always cause suppression in the turbulence intensities. Large particles, $d_p = 3000$ μm, $Re_p \approx \mathcal{O}(1000)$, on the other hand, enhance the turbulence intensities. Hetsroni[6] further examined the effect of the particle Reynolds number on turbulence modulation in the carrier phase. He found that particles with low Reynolds numbers, (i.e., $Re_p \leq 110$) cause suppression of the turbulence, whereas particles with higher Reynolds numbers (i.e., $Re_p \geq 400$) cause enhancement of turbulence due to wake shedding. Gore and Crow[5] summarized the available experimental data and proposed a simple physical model to explain the increase or decrease of turbulent intensity due to particle loading. A critical parameter appears to be the ratio of the particle diameter to the turbulent length scale, d_p/l_e, where l_e is the characteristic length of the most energetic eddy when only one phase is present. They also showed that, at larger values of d_p/l_e (i.e., $d_p/l_e \geq 0.1$), the addition of particles causes an increase in the carrier-phase turbulent intensity, whereas at lower values (i.e., $d_p/l_e \leq 0.1$) the addition causes a decrease. Bachalo et al.,[2] however, found that the ratio of particle diameter to l_e may not be correct. They suggested that the particle characteristic response time is a better parameter to describe the effect of particle loading on turbulence modulation.

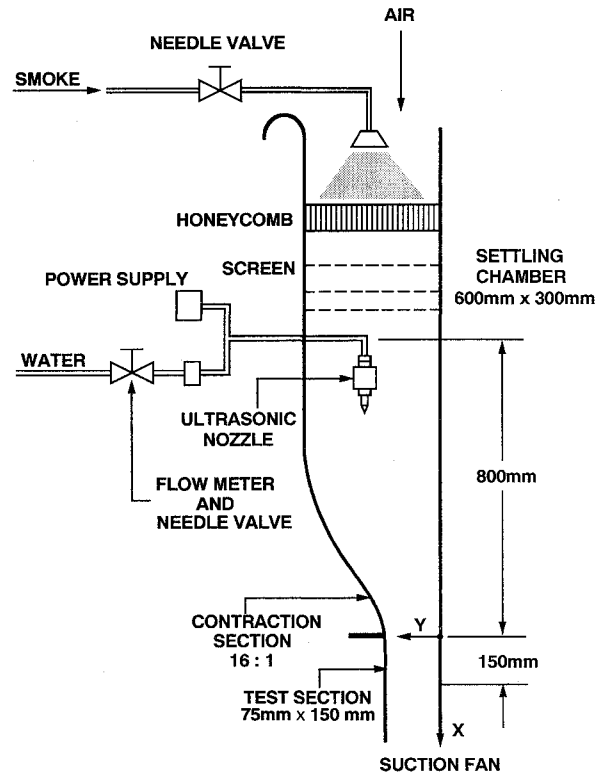

Fig. 1 Schematic of the experimental facility.

In conclusion, the effects of droplet loading on the two-phase turbulent flow as well as the droplet ejection process in the boundary-layer region are relatively underexplored areas in recent literature. This paper will investigate the droplet ejection phenomenon in the boundary layer when the flow is loaded with polydispersed spray for sizes below 110 μm. The effects of the droplet ejection process on the flow, including the change in mean velocity profiles and in turbulence intensities, will also be described in this paper.

II. Experiment Facilities and Measurement Systems

Configuration of the Test Wind Tunnel

A vertical suction-type rectangular duct as shown in Fig. 1 was employed in this study. This rectangular duct was made up of a settling chamber, contraction section, test section, noise reduction chamber, and a suction fan. The contraction ratio of the tunnel is 16:1 with a cross-sectional area of 75 × 150 mm at the test section. The coordinate as shown in Fig. 1 was selected so that the transverse coordinate Y is positive in the area away from the wall, and the streamwise coordinate X is positive in the downstream area with the origin at the entrance of the test section.

Smoke and Droplet Loading System

To distinguish between the velocity of the continuous phase and that of the dispersed droplet phase, the gas flow was seeded with smoke. The seeding smoke particle size was less than 2 μm. The polydispersed water droplets used in this study were generated by a Sono-Tek ultrasonic nozzle with a small cross-sectional area (i.e., 20 mm radius) located at 800 mm upstream from the test section. The arrangement of the ultrasonic atomizing nozzle in the settling chamber is shown in Fig. 1. The cross-sectional area (i.e., 600 × 300 mm) of the settling chamber was large enough to reduce the flow velocity in the settling chamber to less than 1 m/s. The injection velocity of the droplets from an ultrasonic nozzle in the set-

tling chamber was as low as 0.6 m/s. The disturbance due to the existence of the nozzle was negligible because the area blockage ratio of the ultrasonic nozzle in the settling chamber was below 0.7%. The atomizing nozzle used in this study operated at a water flow rate of (25.0 ± 0.75) cc/min with a Sauter mean diameter (SMD) of 53 μm. Since measurements were performed at room temperature (i.e., 25°C), evaporation of water droplets was also considered to be negligible.

Measurement System and Measuring Uncertainty (PDPA)

The two-component phase Doppler particle analyzer (PDPA) (Aerometric model PDP-3200) was used to measure the velocity distribution, particle size, and the number density of the polydispersed droplets in the two-phase boundary layer. The optical system consisted of a transmitter and a receiver module. These packages were affixed to a single base. The transmitter and receiver could also be positioned around the test section to facilitate the required optical access necessary for taking the measurements. Off-axis forward scatter light detection was used. A detailed description of the working principle had been described by Bachalo and Houser.[1] The local mean quantities were averaged by collecting 30,000 samples for every measurement point. The authors considered the statistical significance of the data for each drop size classification. The total samples of each measurement taken were as much as 30,000 which is the instrumentation limit. This provided more than 500 samples for each size class, making the results statistically significant. Gas-phase velocities were determined by seeding small particles, optimizing the PDPA settings to detect small particles, sizing all particles, and then extracting velocity measurements associated with particles measured as being less than 2 μm in diameter. This approach was used previously.[18]

The droplet number density based on drop size was determined from the data measured by PDPA. The data file for PDPA measurements was stored in 50 bins of computer memory, filed in terms of drop size range. For example, the data for drop size class i was summed up from the PDPA measurement in the data bins associated with drop size class i by the following equation.

$$(ND)_i = \frac{\Sigma_i n_i}{\overline{U}_i t A_p} \tag{1}$$

where

$$\overline{U}_i = \frac{\Sigma_i n_i u_i}{\Sigma_i n_i} \tag{2}$$

where u_i and n_i are the velocity and number of the specified drop size, respectively, t is the total sampling time, and A_p is the measuring probe area. A typical drop size range for each class was ±2% of the overall size range in a specific measurement.

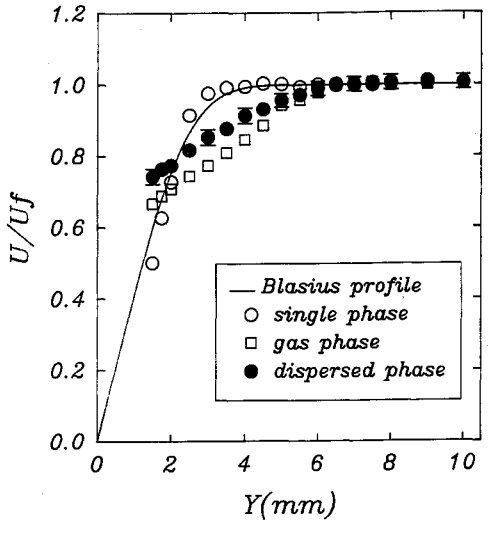

Fig. 2 Velocity profiles of continuous and dispersed phases with and without droplet loading.

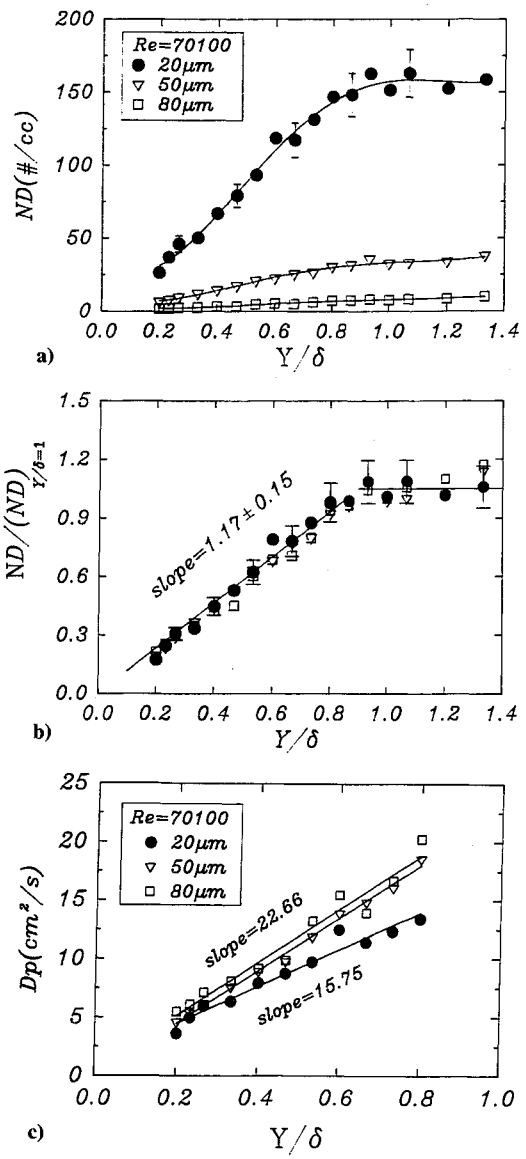

Fig. 3 Droplet number density and dispersion coefficient in the boundary layer: a) number density without normalization, b) normalized number density, and c) droplet dispersion coefficient.

Uncertainties[4,18] in the mean and fluctuating velocities of the continuous phase using the PDPA were within 2% in comparison with the measurements of a pitot tube in the measuring range from 2 to 10 m/s. Repeatabilities in the mean and fluctuating velocities of both phases were also within 2% uncertainty under the test conditions. The variation of number density was within the 10% range in a series of measurements. The uncertainty of the number density was estimated from the mass conservation check of the liquid flow rate measured at X = 145 mm, by comparison with the metered liquid flow rate in the upstream water supply line. Calibration of the monodispersed droplet showed that the error in diameter measurement by PDPA was below 5%. The rejection rates of the PDPA measurement in this study are from 5% in the freestream to 10% near the wall. The phase Doppler particle analyzer was mounted on a three-axis transverse system which permits positioning to within 0.1 mm.

III. Results and Discussion

Experiments were performed at X = 145 mm with freestream velocity 11.2 m/s, corresponding to Reynolds numbers based on the hydraulic diameter, i.e., Re_{D_h} = 70,100. Measurements were carried out at the X = 145-mm position because the test section is only 150 mm, and the authors tried to measure at the position as far from the contraction section as possible to assure a local equilib-

rium condition between phases. Since the drop was seeded 945 mm in the upstream, measurements showed that the number density distribution was uniform in the freestream at the test section position. Results are presented for four drop sizes, 20, 30, 50, and 80 μm, to show the effects of drop size.

Figure 2 illustrates the streamwise velocity distributions for the single-phase flow (i.e., without droplet loading) and for the two-phase flow. Since the velocity profile under the single-phase condition compares favorably with the Blasius profile, it is clear that the boundary layer without droplet loading is essentially laminar in the test flow condition. The laminar boundary-layer thickness calculated at the measured position is 4.0 mm (from the wall to 99% freestream velocity), and the momentum thickness is 0.44 mm under the single-phase condition. Under the two-phase flow condition, the boundary-layer thickness and the momentum thickness of the gas phase (i.e., continuous phase) are 7.5 and 0.84 mm, respectively. It turns out that the Reynolds numbers based on the momentum thickness (i.e., Re_θ) is 317 for the single-phase flow and 605 for the two-phase flow. A paper by Fage and Preston[11] found that the lower limit of Re_θ for a turbulent boundary layer is approximately 320. As is shown in Fig. 2, the velocity profile under the two-phase flow condition deviates from that of the single-phase flow, indicating that droplet loading, like a tripping device, causes flow from the laminar transition to the turbulent. The results also illustrate that the velocity of the single-phase flow is higher than that of the two-phase flow in most of the boundary-layer region. This implies that there is higher momentum and energy transport in the boundary layer due to droplet loading.

Figure 3 shows the dependence of number density distribution on drop size. It can be seen from Fig. 3a that the number density of 20-μm drops is much larger than those of 50- and 80-μm drops. The distribution of the number density is almost uniform at the outer region of the boundary layer, i.e., $Y/\delta > 0.8$. This figure also illustrates that the number densities in the boundary-layer region are lower than those in the freestream region for all drop sizes. Since drop loading is done in the freestream in the beginning, the drops found in the boundary-layer region should be due to drop dispersion from the freestream.

To allow discussion of the drop dispersion phenomenon in the boundary-layer region, the drop number densities for 20, 50, and 80 μm were further normalized by their number densities at $Y/\delta = 1.0$ (see Fig. 3b). It is interesting to see that those three normalized number density distribution curves collapse together, indicating the same dispersion process for all drop sizes. Moreover, the normalized number density distributions can be separated into two regions for all drops, i.e., the linear variation region in the boundary layer (i.e., $Y/\delta \le 1.0$) and the constant distribution region in the freestream (i.e., $Y/\delta \ge 1.0$). The slope of the normalized number density in the linear variation region can be defined as the linear coefficient of the drop number density in the boundary layer Γ of the droplets entrained from the freestream to the boundary layer and can be expressed as

$$\Gamma = \frac{\partial(ND/ND_{Y/\delta=1})}{\partial(Y/\delta)} \tag{3}$$

Analysis of the measured data shows that the linear coefficient of the drop number density Γ is 1.17 ± 0.15 in the boundary layer.

Moreover, the net number flux of the droplets NF can be calculated as

$$NF = (ND) \cdot V_{\text{disp}} \tag{4}$$

where V_{disp} is the droplet dispersion velocity toward the Y direction. Hence, the droplet dispersion coefficient D_p is defined as

$$NF = -D_p \frac{\partial(ND)}{\partial Y} \tag{5}$$

or

$$D_p = \frac{-NF}{\Gamma[(ND)_{Y/\delta=1}/\delta]} \tag{6}$$

Figure 3c illustrates the droplet dispersion coefficient in the boundary layer. It is interesting to find that the variation of D_p in the boundary-layer region is linear. Moreover, the dispersion coefficients of larger droplets (i.e., 50 and 80 μm) are higher than the smaller droplets (i.e., 20 μm). The dispersion coefficient can be characterized by the dispersion velocity and the length scale. The dispersion velocities in the boundary-layer region are higher for the bigger droplets as will be shown in Fig. 9. Hence the dispersion coefficients of the bigger droplets are higher than that of the smaller droplets. As a reference, the slope of the dispersion coefficient are 22.66 and 15.75 for bigger droplets (50 and 80 μm) and smaller droplets (20 μm), respectively.

Further investigation of the droplet motion in the boundary-layer region shows a droplet ejection phenomenon[12] in the boundary layer. Figure 4 illustrates the percentage of droplets ejected from the boundary layer back to the freestream. The percentage of droplets ejected from the boundary-layer region, i.e., droplets with positive transverse velocity, is defined as $P(V^+)$ and is expressed as the following equation:

$$P_i(V^+) = \frac{n_i(V^+)}{N_i} \times 100\% \tag{7}$$

where

$$N_i = n_i(V^+) + n_i(V^-) \tag{8}$$

where $n_i(V^+)$ and $n_i(V^-)$ are the number of drops with positive and negative transverse velocities of specified drop size i, respectively, and N_i is the number of drops with both positive and negative transverse velocities for specified drop size i. As shown in Fig. 4a, $Pi(V^+)$ for 20-μm drops decreases from 15% in the boundary layer to 5% in the freestream, whereas $P_i(V^+)$ for bigger drops remains almost constant in both boundary-layer and freestream regions. This phenomenon has been explained in terms of vortex motion in the boundary-layer region by Rashidi et al.[12]

In an effort to measure the effect of vortex motion on drop ejection in the boundary-layer region, the droplet ejection factor for a specific drop size i in the boundary layer $(\Psi_L)_i$ is defined as the following equation to evaluate the percentage of drops with positive transverse velocity in the boundary-layer region over those in the freestream.

$$(\Psi_L)_i = [P_{BL}(V^+)]_i - [P_f(V^+)]_i \tag{9}$$

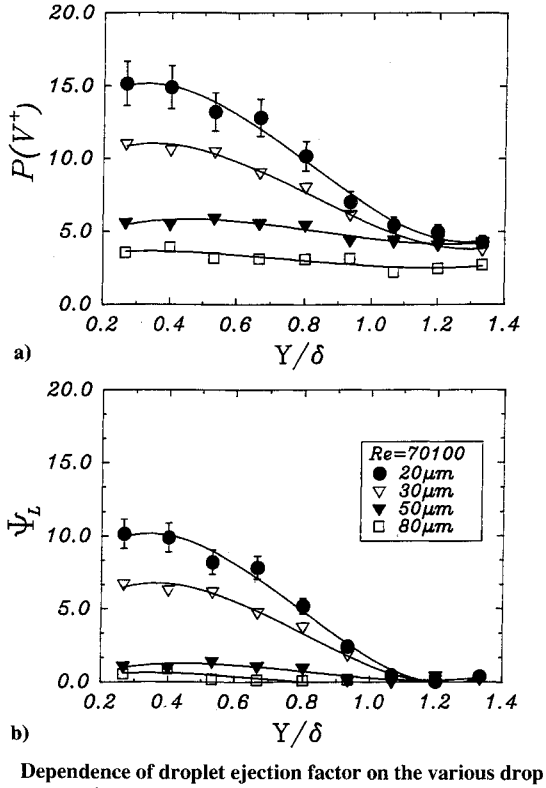

Fig. 4 Dependence of droplet ejection factor on the various drop size: a) percentage of the droplets with positive transverse velocity and b) droplet ejection factor.

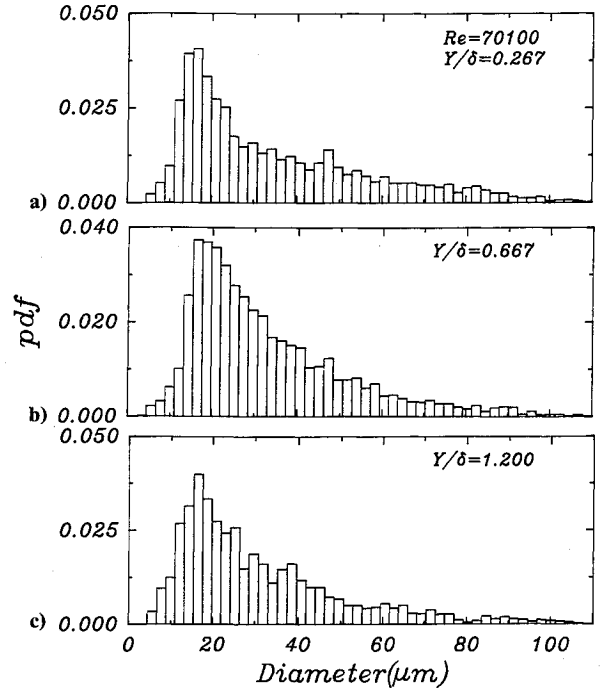

Fig. 5 Distribution of probability density function of drop ejected from the boundary layer region: a) Y/δ = 0.267, b) Y/δ = 0.667, and c) Y/δ = 1.200.

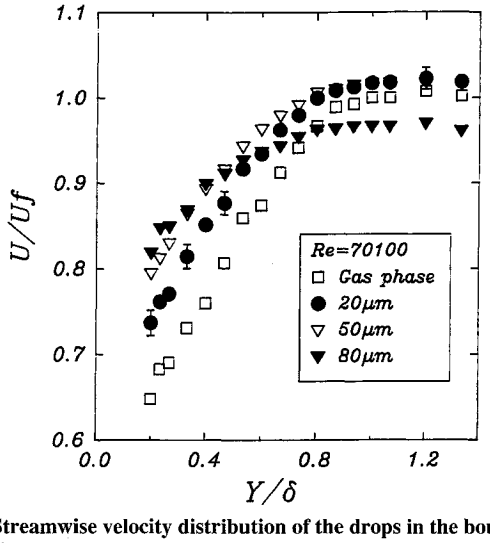

Fig. 6 Streamwise velocity distribution of the drops in the boundary-layer region.

where $[P_{BL}(V^+)]_i$ is the percentage of drops with positive transverse velocity in the boundary-layer region and $[P_f(V^+)]_i$ is that in the freestream. Figure 4b illustrates the droplet ejection factor in the boundary layer for 20-, 30-, 50-, and 80-μm drops. $(\Psi_L)_i$ for larger drops, i.e., 50- and 80-μm drops, is almost zero, implying that the boundary-layer effect on larger drops is insignificant due to their higher inertia. However, $(\Psi_L)_i$ is about 10 and 6% for 20- and 30-μm drops, respectively, indicating that the motion of smaller drops is influenced by the characteristics of the boundary-layer flow. It is suggested that the description of droplet motion in the boundary layer should consider the ejection effect on smaller size drops.

In an attempt to further explain the foregoing results, the probability density function (pdf) for droplets ejected from the wall is depicted in Fig. 5. The pdf histogram of drop ejections is calculated by the following equation:

$$\text{pdf}(d_i) = \frac{n_i(V^+)}{\Sigma_i n_i(V^+)\,\Delta d_i} \tag{10}$$

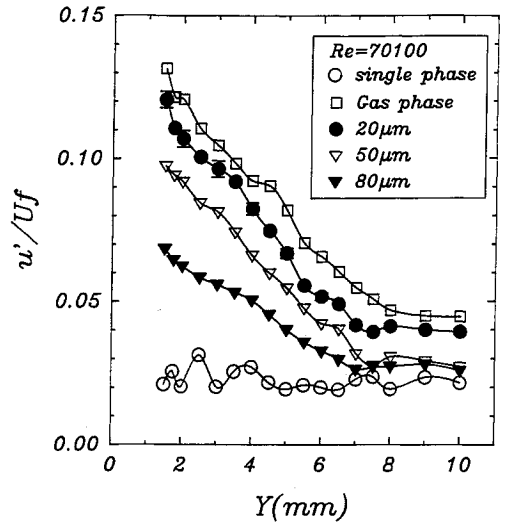

Fig. 7 Streamwise velocity fluctuation distribution of the drops in the boundary-layer region.

where Δd_i is the size interval of each drop size d_i. Figure 5a illustrates the correlation between the pdf and the drop size at Y/δ = 0.267. As shown in this figure, the pdf values decrease as drop size increases from 15 to 110 μm. It is clear that the droplet ejection factor for 20-μm drops is much higher than that of 50- and 80-μm drops, as is consistent with the data shown in Fig. 4. This trend is also found for the pdf's distributions at Y/δ = 0.667 and 1.20 (see Figs. 5b and 5c).

Figure 6 compares the velocity distributions of the gas phase and the dispersed phase. Measurements were carried out as close to the wall as possible, i.e., Y = 1.5 mm or Y/δ = 0.2. It seems that the velocity distribution can be divided into two regions: one is near the wall, i.e., $Y/\delta \leq 0.8$; the other is near the freestream, i.e., $Y/\delta \geq 0.8$. In the outer region of $Y/\delta \geq 0.8$, the velocities of the smaller drops (i.e., 20 and 50 μm) and gas phase are almost the same within the measuring uncertainty. Since the momentum of the drops issued from the nozzle is transferred from the gas phase, the velocity of the larger drops (i.e., 80 μm) is less than that of other drops in this region because of their higher inertia. However, the velocity distributions are quite different in the near-wall region (i.e., $Y/\delta \leq 0.8$). The velocity of the 80-μm drop is the highest in the near-wall region whereas the velocity of the gas phase is the lowest in the same region (see Fig. 6). Similar results were also reported in the literature.[9,15,16] It seems that the viscous effect in the near-wall region is significant and that the influence of this effect on the drop velocities depends on their sizes. The velocity of the larger drops in the near-wall region is higher because of their higher inertia when entrained from the freestream. Furthermore, the higher velocity gradient in the near-wall region implies higher vorticity and vortex motion there. This can be used to explain the higher droplet ejection factor in the boundary-layer region as shown in Fig. 4.

Figure 7 further illustrates the distributions of the turbulence intensities in the flow direction under single- and two-phase flow conditions in the boundary-layer region. The maximum freestream turbulent intensity is 2% for single-phase flow. This is reasonably low in consideration of the limitation of building height on a vertical facility. It is clear that the streamwise velocity fluctuations of the 20-μm drops are larger than those of 50- and 80-μm drops, and the lowest velocity fluctuations occur in the single-phase flow condition. Comparison of Figs. 4 and 7 shows that the region with higher velocity fluctuations near the wall corresponds to the region with a larger number of ejections for the smaller droplets. The velocity fluctuations of the gas phase are larger than those of the single-phase flow, indicating that the flow becomes turbulent under droplet loading. Examination of Fig. 2 also shows that the mean velocity of the gas phase under droplet loading is lower than that of the single-phase flow. Hence, the added turbulent kinetic energy of the gas phase as illustrated in Fig. 7 is mainly converted from mean

Table 1 Skewness and peakness of streamwise velocity pdf at $Y/\delta = 0.267$

	$d_p = 20$ μm	$d_p = 50$ μm	$d_p = 80$ μm
Skewness	−0.220	−1.028	−1.228
Peakness	−0.317	2.025	2.348

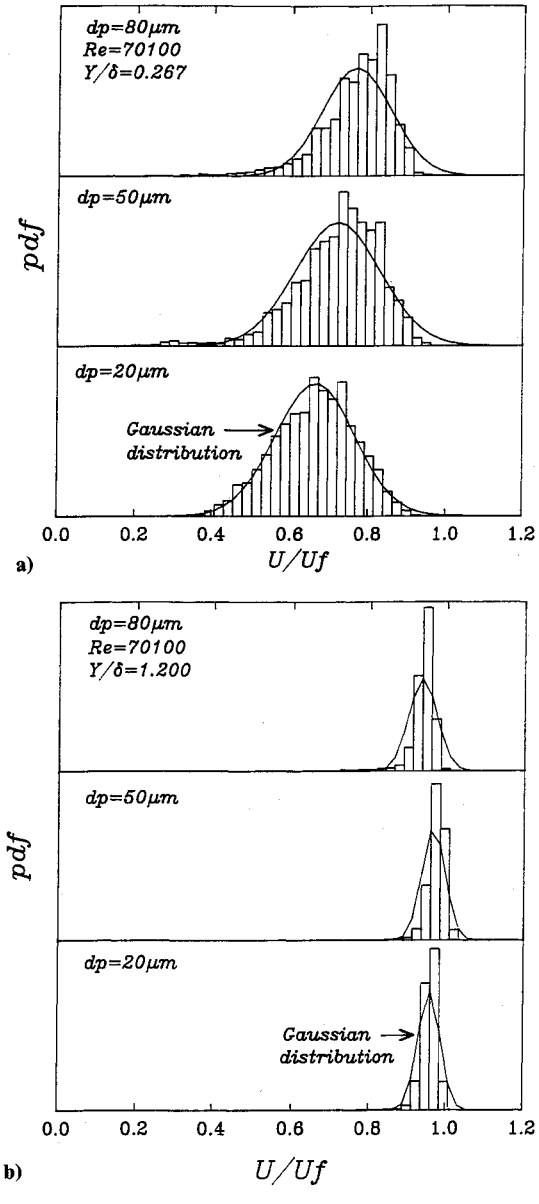

Fig. 8 Histograms of the streamwise velocity probability density functions of 20-, 50-, and 80-μm drops: a) $Y/\delta = 0.267$ and b) $Y/\delta = 1.20$.

kinetic energy. This is consistent with the literature reported by Wang and Liu[17] in 1991. It seems clear that the velocity fluctuations in the gas phase under droplet loading is due to the disturbance caused by the drop motion. This, in turn, results in an increase in the number of ejections in the boundary-layer region.

In an attempt to discuss the physical processes involved in the foregoing results, the velocity probability density functions are further illustrated in Fig. 8. Figure 8a shows the streamwise velocity pdf of 20-, 50-, and 80-μm drops at $Y/\delta = 0.267$. As can be seen from this figure, the most probable value of the distribution function shifts to a higher velocity as the drop size increases from 20 to 80 μm. This indicates that the larger drops possess a greater streamwise velocity than the smaller drops near the wall. Moreover, the 20-μm drops show a wider distribution range, indicating that the streamwise velocity fluctuation of 20-μm drops is higher than larger drops. Table 1 shows the skewness and peakness of the

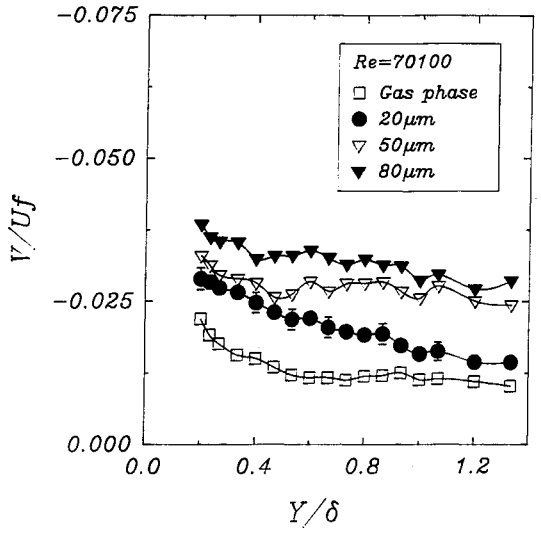

Fig. 9 Transverse velocity distribution of the drops in the boundary-layer region.

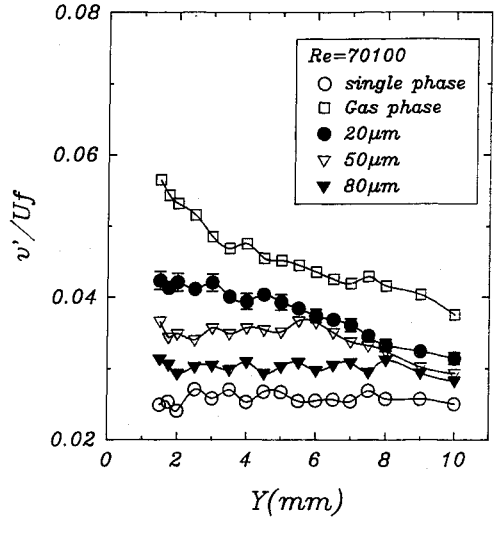

Fig. 10 Transverse velocity fluctuation distribution of the drops in the boundary-layer region.

streamwise velocity for 20-, 50-, and 80-μm drops. The negative skewness of the streamwise velocity increases from −0.22 to −1.23, and the peakness increases from -0.32 to 2.35 as drop size increases from 20 to 80 μm. This indicates that the velocity pdf of smaller drops is almost a Gaussian distribution, similar to that of the gas phase.[15,16] Tsuji and Morikawa[15] used the signals of air and particles to discriminate the velocities of both phases. They also found that, if the discrimination was incomplete, the distribution of the probability density function would show an unusual profile. The higher negative skewness for larger drops is due to their higher inertia. The velocity pdf histograms of 20-, 50-, and 80-μm drops at the outer region of the boundary layer (i.e., $Y/\delta = 1.20$) are different from those near the wall (see Fig. 8b). The most probable value of the distribution function shifts to the lower velocity as the drop sizes increase from 20 to 80 μm, indicating that the streamwise velocity of 80-μm drops is lower than that of others in the main stream. Moreover, the range of the pdf histogram in the main stream is narrower than that in the boundary layer, indicating lower velocity fluctuations in the main stream.

The negative velocity of droplets in the transverse coordinates denotes drop motion into the boundary layer. Figure 9 illustrates the typical transverse velocity profile of the gas phase, and 20-, 50, as well as 80-μm drops at $X = 145$ mm. As shown in this figure, the transverse velocities of the gas phase are lower in both inner and outer edges of the boundary layer. However, the entraining

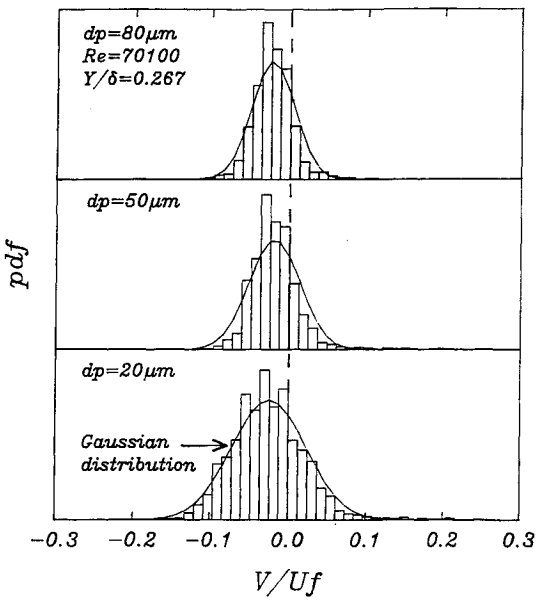

Fig. 11 Histograms of the transverse velocity probability density function of 20-, 50-, and 80-μm drops at $Y/\delta = 0.267$.

velocity slightly increases as the drop size increases because the number of ejections decreases as the drop size increases, as shown in Fig. 4. The transverse velocity fluctuations of the single phase, gas phase, and 20-, 50-, and 80-μm droplets are shown in Fig. 10. This figure shows that the measured maximum transverse velocity fluctuation of the gas phase is $0.057U_f$, about half of that for the streamwise direction. In addition, the fluctuations of various drops are significantly lower than that of the gas phase in the transverse direction. This implies that these drops can not catch up with the turbulent motion of the gas flow in the boundary layer. Similar results were also reported by Rogers and Eaton[14] in 1989.

Figure 11 shows the pdf's distribution of the transverse velocity for 20-, 50-, and 80-μm drops at $Y/\delta = 0.267$ near the wall. The transverse velocity pdf histogram of 20-μm drops shows a wider distribution than that of 50- and 80-μm drops, indicating that the transverse velocity fluctuation of the 20-μm drops is higher than that of 50- and 80-μm drops. This is due to the higher number of ejections for 20-μm drops as shown in Fig. 4. The transverse velocities of the drops cover the negative and positive part in this distribution. Negative and positive transverse velocity represents the transport mechanism of the dispersion and ejection motions in the boundary layer, respectively. In addition, some of the drops near the wall have a positive velocity, indicating an ejection motion of the droplet away from the wall and into the main stream. This is also explained by droplet ejection in the boundary layer, which is described by Rashidi et al.[12]

Results shown in Fig. 4 can also be explained by the transverse velocity pdf shown in Fig. 11. The distribution of the transverse velocity pdf covers both negative and positive parts. The positive transverse velocity represents the ejection motion from the low-speed area near the wall toward the high-speed area near the free-stream. The distribution of the transverse velocity pdf for 20-μm drops covers a wider positive transverse velocity range than that of 50- and 80-μm drops at $Y/\delta = 0.267$, indicating that the droplet ejection factor for 20-μm drops is higher than that of others.

IV. Conclusions

Droplet dispersion and ejection processes in the two-phase boundary layer for drops ranging in size from 20 to 80 μm are described in this paper. The results reveal that the existence of drops in the boundary layer has significant effects on both the velocity profile and the turbulence intensities of the flow. Measurements show that the flow characteristics are controlled by droplet transport processes, i.e., the dispersion of droplets from the freestream to the boundary-layer region and the ejection of droplets from the boundary-layer region to the freestream. Analysis of the data indicates that the normalized number density profiles in the boundary-layer region collapse for all drop size classes. A linear coefficient, 1.17 ± 0.15, could be obtained as further calculating the slope of the normalized number density for droplets from 20 to 80 μm. The slopes of the dispersion coefficients for the larger drops (i.e., 50 and 80 μm) and for the smaller drops (i.e., 20 μm) are 22.66 and 15.75, respectively. These data are very useful to evaluate the dispersion of drops in the two-phase boundary-layer flow. The results also show that the ejection of larger drops is insignificant due to their higher inertia. The droplet ejection factor is 10 and 6% for 20- and 30-μm drops, respectively. This implies that the description of the two-phase boundary layer flow should consider the droplet ejection process of drops in the small size range.

References

[1]Bachalo, W. D., and Houser, M. J., "Phase/Doppler Spray Analyzer for Simultaneous Measurement of Drop Size and Velocity Distributions," *Optical Engineering*, Vol. 23, No. 5, 1984, pp. 583–590.

[2]Bachalo, W. D., Bachalo, E. J., and Sankar, S. V., "Research on Particle Interactions in Two-Phase Turbulent Flows," *Proceedings of the International Conference on Fluid Mechanics*, Beijing, China, 1993, pp. 1130-1141.

[3]Blackwelder, R. F., and Eckelmann, H.,"Streamwise Vortices Associated with the Bursting Phenomenon," *Journal of Fluid Mechanics*, Vol. 94, Oct. 1979, pp. 577–594.

[4]Chang, K. C., Wang, M. R., Wu, W. J., and Liu, Y. C., "Theoretical and Experimental Study on Two-Phase Structure of Planar Mixing Layer," *AIAA Journal*, Vol. 31, No. 1, 1993, pp. 68–74.

[5]Gore, R. A., and Crowe, C. T., "Effect of Particle Size on Modulating Turbulent Intensity," *International Journal of Multiphase Flow*, Vol. 15, No. 2, 1989, pp. 279–285.

[6]Hetsroni, G., "Particle-Turbulence Interaction," *International Journal of Multiphase Flow*, Vol. 15, No. 5, 1989, pp. 735–746.

[7]Kim, H. T., Kline, S. J., and Reynolds, W. C., "The Production of Turbulence near a Smooth Wall in a Turbulent Boundary Layer," *Journal of Fluid Mechanics*, Vol. 50, Nov. 1971, pp. 133–160.

[8]Kline, S. J., Reynolds, W. C., Schraub, F. A., and Runstadler, P. W., "The Structure of Turbulent Boundary Layer," *Journal of Fluid Mechanics*, Vol. 30, Dec. 1967, pp. 741–773.

[9]Lee, S. L., and Durst, F., "On the Motion of Particles in Turbulent Duct Flows," *International Journal of Multiphase Flow*, Vol. 8, No. 2, 1982, pp. 125–146.

[10]Luchik, T. S., and Tiederman, W. G., "Timescale and Structure of Ejections and Bursts in Turbulent Channel Flows," *Journal of Fluid Mechanics*, Vol. 174, Jan. 1987, pp. 529–552.

[11]Fage, A., and Preston, J. H., "On Transition from Laminar to Turbulent Flow in the Boundary Layer," *Proceedings of the Royal Society of London*, Ser. A, Vol. 178, 1941, pp. 201–227.

[12]Rashidi, M., Hetsroni, G., and Banerjee, S., "Particle-Turbulence Interaction in a Boundary-Layer," *International Journal of Multiphase Flow*, Vol. 16, No. 6, 1990, pp. 935–949.

[13]Robinson, S. K., "Coherent Motions in the Turbulent Boundary Layer," *Annual Review of Fluid Mechanics*, Vol. 23, 1991, pp. 601–639.

[14]Rogers, C. B., and Eaton, J. K., "Particle Response and Turbulent Modification in a Flat Plate Turbulent Boundary Layer," ASME, FED-Vol. 80, *Turbulence Modification in Dispersed Multiphase Flows*, American Society of Mechanical Engineers, 1989, pp. 15–22.

[15]Tsuji, Y., and Morikawa, Y., "LDV Measurements of an Air-Solid Two-Phase Flow in a Horizontal Pipe," *Journal of Fluid Mechanics*, Vol. 120, July 1982, pp. 385–409.

[16]Tsuji, Y., Morikawa, Y., and Shiomi, H., "LDV Measurements of an Air-Solid Two-Phase Flow in a Vertical Pipe," *Journal of Fluid Mechanics*, Vol. 139, Feb. 1984, pp. 417–434.

[17]Wang, M. R., and Liu, Y. C., "Transport Mechanism in Two-Phase Boundary Layer," *8th National Conference on Mechanical Engineering*, CSME, Taipei, Taiwan, ROC, 1991, pp. 119–126.

[18]Wang, M. R., and Huang, D. Y., "Droplet Dynamic Near the Wall in a Vertical Rectangular Duct," *Journal of Fluids Engineering*, Vol. 116, No. 2, 1994, pp. 349–353.